*Journal of Structural Geology*, Vol. 4, No. 4, pp. 411 to 428, 1982
Printed in Great Britain

0191-8141/82/040411-17 $03.00/0
Pergamon Press Ltd.

# The relationship between foliation and strain: an experimental investigation

B. E. HOBBS

Department of Earth Sciences, Monash University, Clayton, Victoria 3168, Australia

W. D. MEANS

Department of Geological Sciences, State University of New York at Albany, Albany, NY, U.S.A.

and

P. F. WILLIAMS

Department of Geology, University of New Brunswick, Fredericton, New Brunswick E3B 5A3, Canada

(*Received* 13 *October* 1981; *accepted in revised form* 21 *May* 1982)

**Abstract**—A multilayered salt/mica specimen with embedded strain markers was shortened to produce a fold and the distribution of strain was subsequently mapped out over the profile plane. On a fine scale the initial foliation, which is parallel to the undeformed layers, is folded by tight kinks to produce two new foliations; one is defined by the preferred orientation of kink boundaries and the other by the preferred orientation of (001) of mica. In the hinge region of the fold the first of these new foliations is parallel to the local $\lambda_1\lambda_2$-principal plane of strain whereas the preferred orientation of mica is bimodal and is symmetrical about the $\lambda_1\lambda_2$-plane. Elsewhere the two new foliations are not parallel to the principal plane of strain and angular divergencies of up to 30–35° are measured. If a March model with initial random mica orientation is assumed for the development of mica preferred orientation then the correct value of strain is predicted but the orientation of the principal plane of strain can be grossly in error. A theoretical analysis of the angular relationships to be expected between kink boundaries and the $\lambda_1\lambda_2$-plane of strain confirms that for the type of geometries experimentally developed, large divergences of up to 35° should be common. In rocks where the foliation has developed by processes similar to those recorded here, large angular divergencies between the foliation and the $\lambda_1\lambda_2$-principal plane of strain should be expected as the rule.

## INTRODUCTION

THE PAST 15 years has seen an emphasis on investigating the distribution of strain in deformed rocks and in relating this distribution to the types of structures observed in various parts of folds. From many of these studies, there has emerged the general contention that foliations such as slaty cleavage and schistosity are parallel to a principal plane of the finite strain ellipsoid, normal to the principal axis of shortening (see for instance, Ramsay & Graham 1970, Siddans 1972, Wood 1974, Wood *et al.* 1976). This of course supports the much earlier view expressed by Sorby (1853) but (see Bayly 1974, Williams 1976, 1977, Means 1977, Knipe & White 1977) some doubts have been cast on the general truth of this relationship. The objections raised are more specific than those voiced in the past by authors such as Becker (1893) who claimed that slaty cleavage formed parallel to a plane of maximum shear strain.

The objections centre around the observation that it is not possible, in a general non-coaxial deformation history, for a plane of material particles to remain parallel to the $\lambda_1\lambda_2$-plane of strain throughout the deformation history. (In this paper $\lambda_1$, $\lambda_2$ and $\lambda_3$ are the maximum, intermediate and minimum principal quadratic elongations.) Only in coaxial deformation histories is this strictly possible (see Williams 1976).

Many authors (for example, Darwin 1846, Sorby 1853, Harker 1885, Hoeppener 1956, Plessmann 1964, Talbot 1965, Williams 1972, 1976, 1977, Etheridge & Lee 1975, Means 1977, Knipe & White 1977) have pointed out that slaty cleavage does not normally consist simply of a penetrative preferred orientation of mica flakes parallel to the cleavage plane. In general, a discontinuous structure has developed consisting of domains of strongly and weakly deformed material, of domains of slightly different mineralogy, of fine-scale metamorphic differentiation zones, or of combinations of these features. Similarly, crenulation cleavage and schistosity may be defined by material discontinuities or compositional variations rather than by the simple regular distribution of oriented micas. The fact that these foliations are primarily defined by discontinuities and domains means that for general non-coaxial deformation histories, it is not possible for the foliation to remain parallel to the $\lambda_1\lambda_2$-principal plane of strain throughout the deformation history, although the observation is true that many material planes must rotate towards this principal plane of strain during increasing deformation. The exception to this argument would arise if diffusional or mechanical adjustments could take place at a sufficiently fast rate that the foliation remained parallel to the $\lambda_1\lambda_2$-plane, no matter whether the deformation history was coaxial or not.

Related to this exception is the idea that the foliation

may not be parallel to a principal plane of strain on a fine scale but that there is nevertheless something inherent in the mechanism of formation of foliations such as slaty cleavage that ensures that the foliation is always parallel to the principal plane of mean strain no matter what the deformation history. This argument admits that there may be small domains of differing strains so that the deformation is inhomogeneous on a fine scale and there may even be shear displacements parallel to the foliation on this scale; locally, the foliation is not coincident with a principal plane of strain, but so the arguments go, on a scale where the deformation can be considered to be homogeneous, the foliation would always remain parallel to the $\lambda_1\lambda_2$-principal plane of mean strain, there being something (as yet undefined) in the mechanism of formation that ensures that this is so.

Foliations defined by the boundaries of domains in which the strain is different include crenulation cleavage as the obvious example but many slaty cleavages are of this type also; in fact the difference between crenulation cleavage and many slaty cleavages is apparently only one of scale (see Knipe & White 1977, Weber 1981). Other types of domainal slaty cleavage, especially those defined by fine-scale metamorphic differentiation are relevant here also. The above argument is particularly relevant to the foliation described in this paper and is considered further in the discussion section where it is shown that it requires very special geometrical conditions for the $\lambda_1\lambda_2$-principal plane of mean strain to coincide with the domain boundaries that define foliations of this type.

Thus, if it happens to be true that foliations are strictly parallel to the principal plane of mean strain for all rocks, then this implies rather special features of the mechanism of foliation development or of the deformation histories in rocks such that nearly coaxial histories are common, and it is important to resolve the issue. As a step toward resolution we have produced axial-plane foliations experimentally such that the distribution of strain in various parts of a folded specimen is accurately known. In this paper we compare the orientation of the foliation with the known distribution of strain in a representative specimen. In a subsequent paper (Means *et al.* in press) the orientation and intensity of a foliation is discussed in terms of strain history.

## EXPERIMENTAL PROCEDURE

The specimen is a twelve-layer assembly of salt and salt–mica layers. There are two salt layers in the middle and five salt–mica layers on either side (Fig. 1). Individual layers were made by dry compaction of powders in a rectangular pellet press at a pressure (friction neglected) of 360 MPa. The resulting slabs of material were 7.8 cm long, 1.0 cm wide, and of various thicknesses of the order of 0.25 cm. The salt is a table salt ground to reduce the coarser particles to about 100 $\mu$m. The mica is a synthetic fluorine phlogopite with larger flakes about 500 $\mu$m in diameter. This is the same salt–mica mixture used by Means & Williams (1972) and Williams *et al.* (1977). The salt–mica layers acquire a strong foliation parallel to layer boundaries during compaction. It is defined by preferred orientation of mica flakes and the long axes of flattened salt grains and grain aggregates, as described more fully in Williams *et al.* (1977).

Following compaction, the layer thicknesses were measured at the centre and ends of each layer and thirty one evenly-spaced marker lines were applied to the broad sides of each layer by rubber stamp. The marker lines run parallel to the intermediate dimension of each layer, and parallel to the eventual fold axis. One side of each layer was marked with red ink and the other side with green ink. The layers were stacked to form a specimen such that each interface between layers carried red markers attached to one layer and coincident green markers attached to the other layers. This made it possible in the folded specimens to recognize sites of interlayer slip (from separation of the red and green markers), and to calculate intralayer strains free of the effects of interlayer slip.

Once marked and stacked, the twelve layers comprising a specimen were fitted into a pre-cast, thick lead jacket, mounted between oversize pistons, and enclosed in a rubber jacket. The arrangement of pistons, specimen and jackets is illustrated in Means (1975), with the slight modification that we used thin lead pads at the specimen/piston interfaces in the present work, to promote large strain of the specimen along its entire length.

The deformation was carried out at 103 MPa confining pressure, room temperature and at a strain rate of $1.2 \times 10^{-4}\,s^{-1}$. The specimen as a whole was shortened by about 50%. It extended principally in a direction normal to the original plane of the layering, that is perpendicular to the hinge lines of the folds. There were also substantial extensions, up to 20%, parallel to the hinge lines of the folds, especially in the centre of the specimen. The two exterior profile planes of the specimen thus bulged out symmetrically after deformation. From the overall symmetry of the deformed specimen it was inferred that the central profile plane of the folded specimen should contain the local $\lambda_1$ and $\lambda_3$ directions at all points in the profile plane. The specimen dimensions parallel to the fold axis were measured at fifteen points distributed over the profile faces and the specimen was sawn in two along the central profile plane, for investigation of the two-dimensional strain field in this plane and associated foliations.

## STRAIN DISTRIBUTION

The marker lines stamped on the layers intersect the central profile plane in an array of marker points (Fig. 1a). There are in principle 744 points and they define the corners of 720 small triangular regions for each of which the two-dimensional strain can be calculated. In fact a few of the points are missing, on account of incomplete printing by the rubber stamp or subsequent destruction by deformation, so that strain for a few triangles could not be determined.

The first step in the strain determinations was assign-

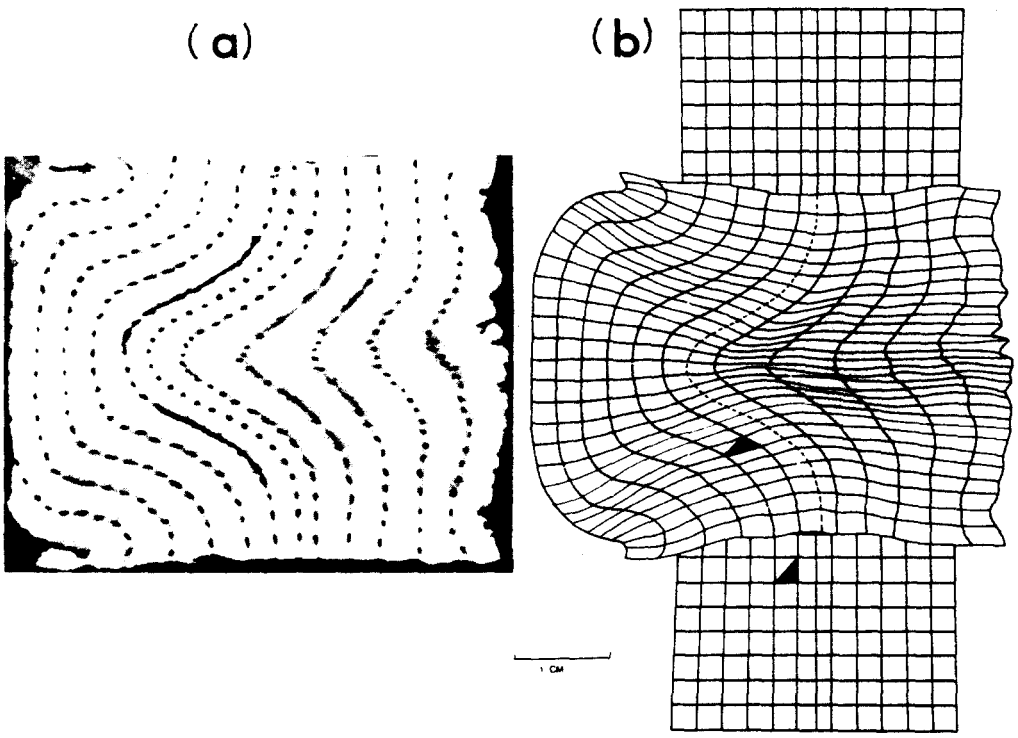


Fig. 1. (a) Cross-section of specimen showing deformed positions of markers. (b) Undeformed and deformed grids on specimen. The marked triangle is typical of those used to calculate strains.

ment of coordinates to each marker point in the deformed and undeformed states. For the deformed state this was done by digitizing a map of the markers prepared from an enlarged version of Fig. 1(a), with binocular inspection of the sawn surface to distinguish the red from the green spots. Coordinates in the undeformed state could not be measured directly from the undeformed specimen because the specimen was not in its final 'undeformed' configuration (i.e. the configuration immediately prior to layer-parallel shortening) until it had been placed in its lead jacket and subjected to confining pressure. The confining pressure collapsed the lead jacket tightly around the specimen and welded the layers into a solid block. Since the layers as compacted and measured were 1–6% thicker at their ends than at their centres, some small deformation of the layers must accompany pressurization. The assumptions made in calculating the undeformed coordinate are (1) that the middle interface between the two salt layers became planar during pressurization and (2) that the spacing of markers measured parallel to the middle interface was not affected by pressurization. These assumptions are consistent with results of tests in which a specimen was brought up to pressure and back down again without further deformation. Figure 1(b) shows the calculated undeformed shape of the specimen along with a profile view of its deformed shape.

Calculation of the principal strains $\lambda_1$ and $\lambda_3$ assumes that the strain field is homogeneous on the scale of each triangle. It proceeds by use of the fact that if the extensions are known for two lines that are perpendicular in the deformed state, and the shear strain is known for one of them, the two-dimensional strain is fully defined. The two lines used here for each triangle were AB and CD (Fig. 2). AB is a line connecting two strain markers on either side of a layer that were opposite one another in the undeformed state. CD is a line perpendicular to AB in the deformed state, with length equal to the altitude of the triangle, where AB is the base.

Using the deformed and undeformed coordinates of markers A, B and C, the quadratic elongations $\lambda_{AB}$ and $\lambda_{CD}$ were calculated, as well as the shear strain $\gamma_{AB}$, from which $\lambda'_{AB}$, $\lambda'_{CD}$, and $\gamma'_{AB}$ were obtained, where

$$\begin{aligned} \lambda'_{AB} &= 1/\lambda_{AB} \\ \lambda'_{CD} &= 1/\lambda_{CD} \\ \gamma'_{AB} &= \gamma_{AB}/\lambda_{AB}. \end{aligned} \tag{1}$$

These three quantities are sufficient to define two invariants of the finite strain, I and II, where:

$$\begin{aligned} \mathrm{I} &= \lambda'_{AB} + \lambda'_{CD} \\ \mathrm{II} &= (\lambda'_{AB})(\lambda'_{CD}) - (\gamma'_{AB})^2. \end{aligned} \tag{2}$$

Finally, the magnitudes of the principal quadratic elongations were found from the invariants by

$$\begin{aligned} \lambda_1 &= \frac{2}{\mathrm{I} - (\mathrm{I}^2 - 4\mathrm{II})^{1/2}} \\ \lambda_3 &= \frac{2}{\mathrm{I} + (\mathrm{I}^2 - 4\mathrm{II})^{1/2}} \end{aligned} \tag{3}$$

(Ramsay 1967, p. 82). The orientation of the $\lambda_1$ direction is obtained from

$$\theta' = \sin^{-1}\left[\frac{\lambda'_{AB} - \lambda'_1}{\lambda'_3 - \lambda'_1}\right]^{1/2}, \tag{4}$$

where $\theta'$ is the angle in the deformed state between the line AB and the $\lambda_1$ direction.

The calculations were carried out for the four sets of triangles shown in Fig. 3. This is a redundant procedure since calculations in the first and second sets of triangles or in the third and fourth sets fully define the strain field. However, it is useful because differences in the two sets of results provide a check on estimated errors in the strain

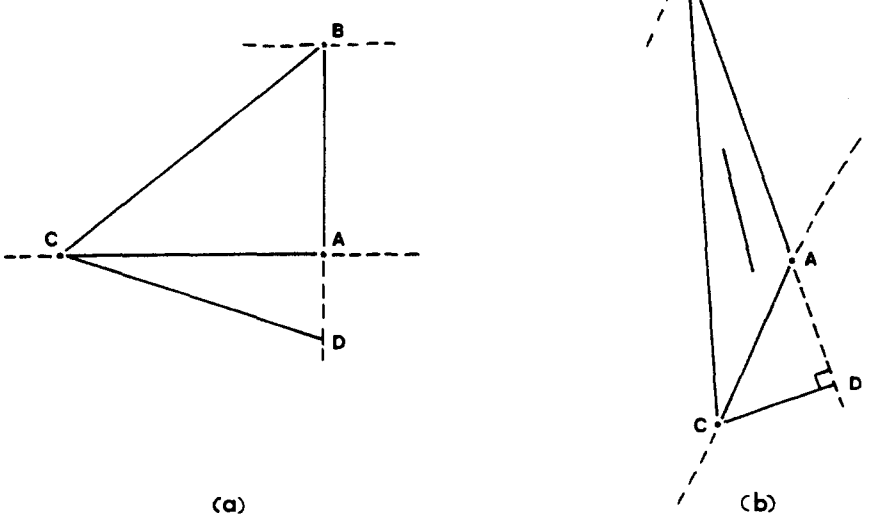


Fig. 2. Undeformed (a) and deformed (b) triangles. The line drawn in the centre of the deformed triangle in (b) shows the calculated orientation of the direction of $\lambda_1$.

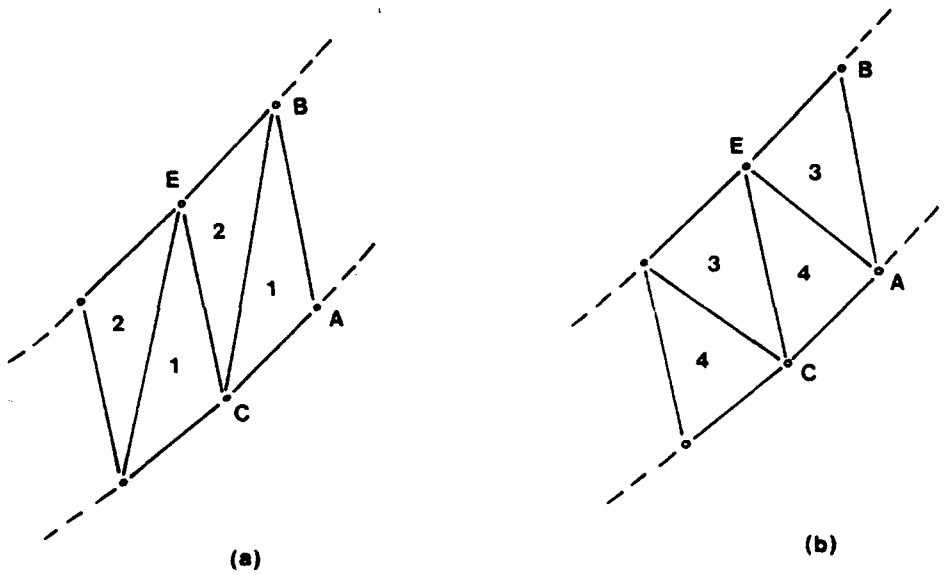


Fig. 3. A portion of one of the layers, showing two alternative ways of subdividing it into triangular regions for the strain calculations. Triangles of sets 1 and 2 were used for subsequent plots in this paper.

calculations, as discussed in the next section. The results that follow are for calculations in the first and second sets of triangles (Fig. 3a) unless otherwise noted.

Figure 4 is a plot showing the deformed array of markers and the local direction of $\lambda_1$ for each triangle where all three markers were readily identifiable in the deformed state.

Figure 5 is a contour map of the magnitude of the greatest-principal strain, plotted as the square root of $\lambda_1$. Following Truesdell & Toupin (1960, p. 255) we refer to the square root of a quadratic elongation as a stretch (see also Hobbs 1971, p. 334; Means 1976, p. 134). The stretch is the ratio of the length of a line in the deformed state to

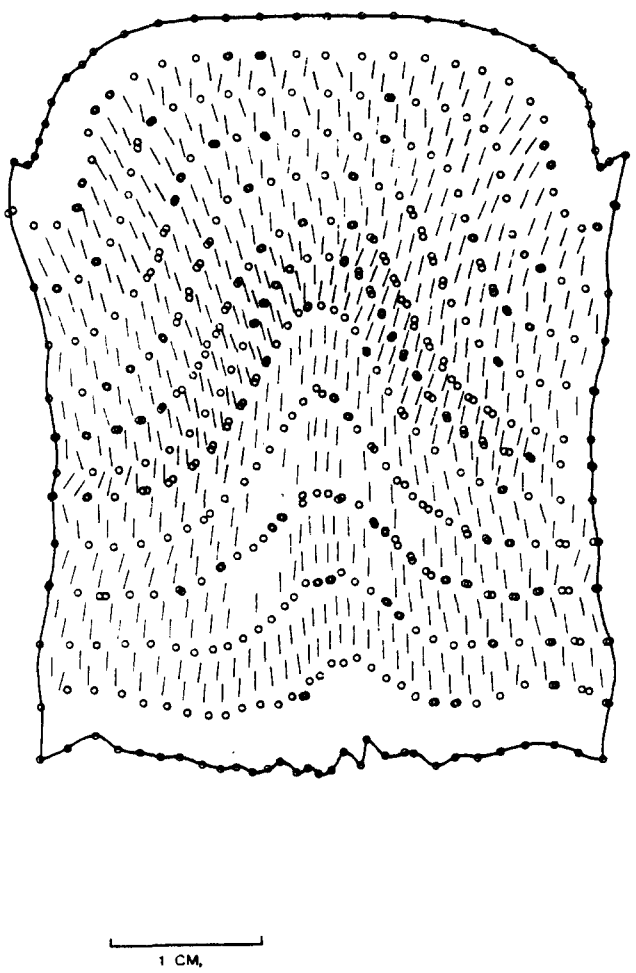


Fig. 4. Calculated orientations of the $\lambda_1$ direction in the central profile plane of the specimen. (Circles are marker points of Fig. 1a).

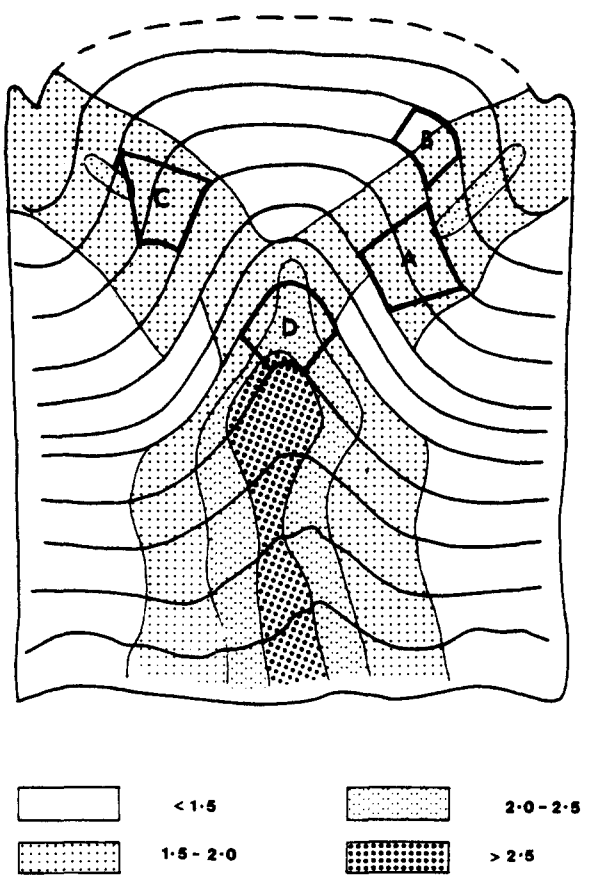


Fig. 5. Contour map showing magnitudes of $\sqrt{\lambda_1}$ (numbered in key) in the central profile plane. A, B, C and D are areas studied in greater detail later in the text.

its length in the undeformed state, and the stretches indicated in Fig. 5 thus show the lengths of the long axis of a strain ellipse derived from a circle of unit diameter.

*Calculation of the principal strain $\lambda_2$ and volume changes*

Figure 6(a) is a map of the deformed specimen showing the fifteen points at which its thickness was measured parallel to the fold axis. From these measurements a thickness was assigned to each triangle by linear interpolation between the three measured thicknesses that were closest to each triangle. The intermediate principal strain was then calculated for each triangle, taking the initial thickness of the specimen as uniform and equal to 1.9 cm. The resulting values of the intermediate principal strain, expressed as stretches, are contoured in Fig. 6(b). The volumetric strain or dilation $\Delta$ is calculated from

$$\Delta = 1 - \sqrt{\lambda_1 \lambda_2 \lambda_3} \qquad (5)$$

and is illustrated in Fig. 6(c).

*Errors in strain determinations*

The main source of error in the two-dimensional strain calculated for each triangle is uncertainty in the measured positions of the markers in the strained state. The markers have finite size and they are thus distorted by the deformation. Some are quite smeared out as suggested in Fig. 1(a). However, the situation is not as bad as the black and white photograph suggests. When the photograph is compared with the original specimen surface, viewed through a low-power microscope, it is possible to resolve most of the smeared out black markers in the photograph into separate red and green parts and to locate the centre of each separate part within $\pm$ 0.5 mm on a 20 $\times$ 25 cm enlargement of the photograph. For some markers this was not possible, because they were too severely deformed or missing altogether, and for triangles involving such markers, no strain quantity is shown in Fig. 4 or other plots.

The errors in marker locations lead to maximum uncertainty of $\pm$ 10% in lengths calculated across the layers and to maximum uncertainty of $\pm$ 20% in lengths calculated parallel to the layers (where the spacing of markers is commonly smaller and the percentage error correspondingly higher). The calculated values of the principal stretch $\sqrt{\lambda_1}$ which is essentially a length across the layers, are therefore expected to be in error by up to about $\pm$ 10% and the calculated principal stretch $\sqrt{\lambda_3}$ which in the worst cases corresponds to a length parallel to the layers, may be in error by up to $\pm$ 20%. These errors in the principal stretches correspond to errors of $\pm$ 20% and $\pm$ 40% in the principal quadratic elongations $\lambda_1$ and $\lambda_3$. With such errors possible in the quadratic elongations, the maximum errors in the calculated orientations of the $\lambda_1$ or $\lambda_3$ directions within the areas we want to consider in detail, are $\pm$ 5°.

It is possible to check these estimates of errors in several ways. First, it can be noted that the $\lambda_1$ directions in Fig. 4 tend to vary smoothly from one triangle to the next in a given layer. Where wild fluctuations are seen, i.e. near the centre of the second-to-top layer in Fig. 4, they correspond to areas where the strain is small and the microstructure indicates that the strain field is heterogeneous on the scale of a single triangle (e.g. the foliation is kinked on a scale comparable with the size of a triangle).

Second, strain calculations done in overlapping triangles of the four sets can be compared with one another. Thus, for example, if region ABEC in Fig. 3 were homogeneously deformed and if the positions of the markers ABEC were measured without error, the strains determined for triangles 1, 2, 3 and 4 would be exactly equal. Departures from exact equality would reflect departures from homogeneous deformation and/or errors in positions measured for the markers and, thus, provide an independent indication of the maximum possible errors arising from bad measurements. This comparison

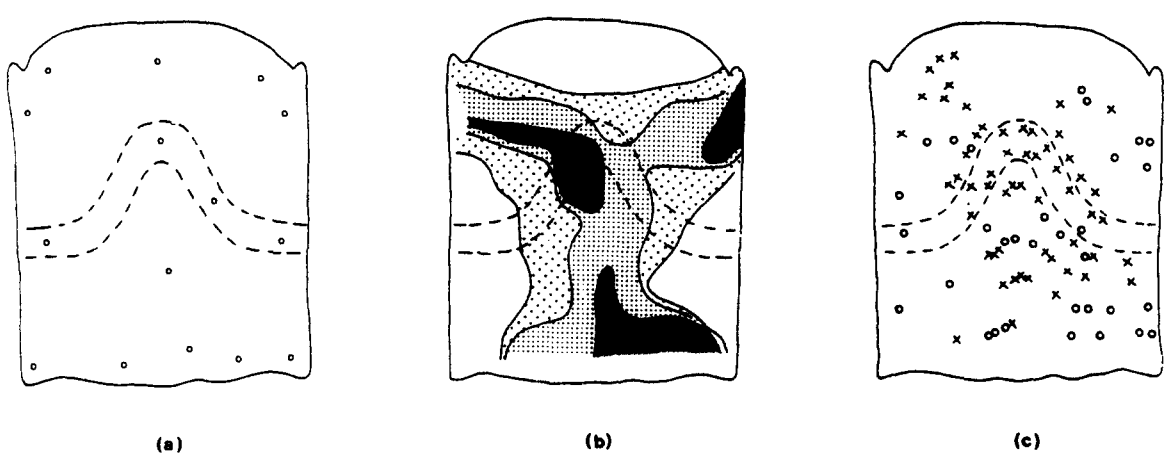


Fig. 6. Profile views of the specimen showing aspects of the three-dimensional strain calculations. (a) Fifteen points where the dimension of the specimen parallel to the fold axis was measured, and at which the principal strain $\sqrt{\lambda_2}$ is most accurately known. (b) Contours showing the calculated values of $\sqrt{\lambda_2}$ elsewhere: shaded, $\sqrt{\lambda_2} > 1.2$ parallel to the fold axes; small dots, $\sqrt{\lambda_2}$ = 1.15–1.2; large dots, $\sqrt{\lambda_2}$ = 1.1–1.15. (c) Extreme values of volumetric strain. Crosses: points at which calculated volume decrease exceeds 20%. Circles: points at which calculated volume increase exceeds 10%.

was made for the 120 triangles of sets 1, 2, 3 and 4 comprising the fourth layer from the top of the specimen in Fig. 1(a). For any given set of four triangles the maximum departure of $\sqrt{\lambda_3}$ was $\pm$ 30% from its value, and the $\lambda_1$ directions were off the mean value for any group of four triangles by a maximum of $\pm$ 10°. Considering that part of these variations is certainly due to inhomogeneity in the deformation, this is considered to confirm the estimates made earlier of the accuracy of the strain measurements, in particular the statement that $\lambda_1$ orientations should be good to $\pm$ 5° for each individual triangle.

Where the $\lambda_1$ orientation is read from Fig. 4, not for individual triangles, but for groups of adjacent triangles with concordant $\lambda_1$ orientations, the $\lambda_1$ direction is most accurately defined, perhaps to $\pm$ 3°.

Errors in measurement of the dimensions of the specimen parallel to the fold axis are considered to be $\pm$ 5% and this leads to errors of similar magnitude in the calculated values of $\sqrt{\lambda_2}$ When this error is combined with errors of $\pm$ 10% and $\pm$ 20% for $\sqrt{\lambda_1}$ and $\sqrt{\lambda_3}$, respectively, errors of up to 40% are possible in the calculated volume changes and volumetric strains.

In view of the high compaction of this experimental material prior to deformation, it is not considered that the large dilations given in Fig. 6(c) are realistic; dilations of perhaps 5–10% would seem more reasonable. The large magnitudes of the calculated errors in the dilation provide a possible explanation.

## MICROFABRIC

The initial foliation in the specimen is modified during the deformation to produce a new preferred orientation of mica and salt aggregates. The precise structures produced depend on the amount of strain locally and this in turn depends on position relative to the fold. The description below is in terms of the various areas delineated in Fig. 5.

### *Low strain areas (magnitude of $\sqrt{\lambda_1} < 1.5$)*

In the regions of relatively low strain close to the deforming pistons and in the fold closure on the convex side of the folded salt layer, there are two sets of kinks in the initial schistosity. They are fairly open kinks with axial surfaces approximately parallel to the piston faces and to the axial surface of the large fold. There are also less numerous kinks with their axial surfaces approximately parallel to bedding. These are the kinks formed during compaction of the specimen (see Williams *et al.* 1977). They are still tight structures but are not as tight as in the undeformed starting material. This is due to the shortening that has occurred during deformation parallel to their axial surfaces. Locally, these two generations of folds cause complicated interference patterns.

### *High strain areas (magnitude of $\sqrt{\lambda_1} > 1.5$)*

In the high strain area of the fold closure on the concave side of the salt layer, the initial mica foliation is folded into a series of asymmetric, or locally symmetric, kinks. The kinks generally have interlimb angles between 30 and 60°. The symmetric kinks are close to the trace of the axial surface and the asymmetric kinks have the sense of asymmetry of normal parasitic folds. The kinks occur on all scales from folds involving tens of mica grains to intra-crystalline structures. Their axial surfaces define a divergent fan with respect to the larger fold. The asymmetric kinks have long limbs that are several times as long as their short limbs. This, combined with their tightness, means that they define a strong orientation maximum for (001) of mica which has the normal bedding–cleavage relationship of an axial-plane foliation.

In the high strain areas on the convex side of the salt layer, the initial foliation is deformed in much the same manner as on the concave side but the kinks are less tight. The interlimb angle tends to be around 60° and the difference in the length of limbs is not as great. The axial surfaces of kinks define a convergent fan with respect to the larger fold.

The new foliation developed in this specimen has all of the characteristics of the foliation described in Williams *et al.* (1977).

The orientations of the axial surfaces of small kinks are plotted in Fig. 7(a); these orientations are compared to the relevant orientations of the $\lambda_1\lambda_2$-plane of the finite strain ellipsoid (taken from Fig. 4), in Fig. 7(b). Departures in orientation of up to 32° between a kink boundary and the local $\lambda_1\lambda_2$-plane are noted especially within the higher strain areas on the convex side of the fold. As is to be expected, in the symmetrical environment of the fold hinge there are no angular departures between the kink boundaries and the $\lambda_1\lambda_2$-planes; the distribution of departures is systematic with respect to the fold.

A little more detail is given in Fig. 8 which shows histograms of kink plane orientations for the four regions around the fold labelled A, B, C and D in Fig. 5. In regions A, B and D the mean orientation of kink planes is parallel to the local orientation of the $\lambda_1\lambda_2$-plane of the finite strain ellipsoid within the accuracy of measurement, although it is important to note that individual kink planes in these regions need not be parallel to the local $\lambda_1\lambda_2$-plane. Within area C, however, a divergence of approximately 15° between the mean orientations of kink planes and the local $\lambda_1\lambda_2$-plane is evident and local divergences of up to 28° are developed.

Histograms showing the frequency distribution of angles between the initial foliation and kink planes as shown in Fig. 9 for the four areas A, B, C and D of Fig. 5 and details of the kink geometry within these areas are summarized in Table 1.

### *Conjugate shears*

Some regions of the fold are traversed by shear zones that form a conjugate pair. No actual intersections of

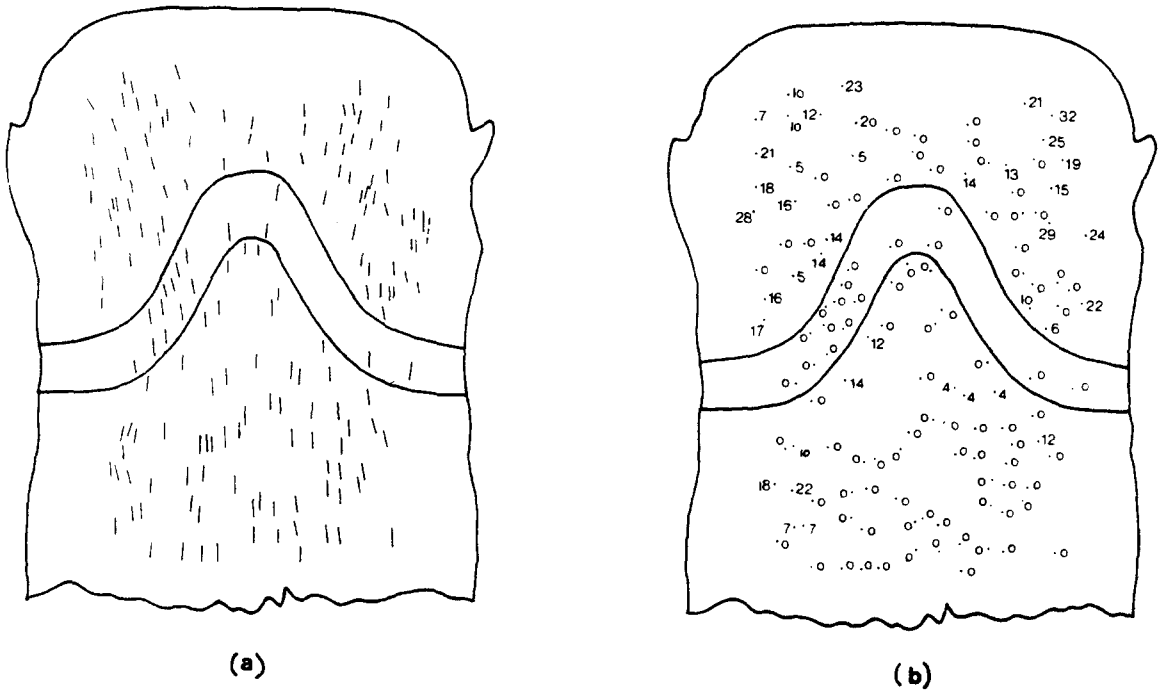


Fig. 7. (a) Orientations of axial surfaces of kinks in the deformed salt/mica regions and of foliation in the central salt layer. (b) Measured angles between the traces of kink boundaries or salt foliation and $\lambda_1\lambda_2$-principal planes of strain.

these zones are observed; as they approach one another, one or both die out. These zones are defined in part by dark hairlines that are commonly stained by the red dye used for the strain markers. The red dye, in particular, continues to diffuse out from the central red line of application for several days after imprint forming a light but noticeable smear twice the diameter of the initial imprint. The fact that this dye diffuses relatively very large distances along the shear zones, means that these zones are regions of great permeability and are presumably associated with relatively large dilations. More generally however, the shear zones are defined by a difference in the orientation of the foliation; they constitute a small open flexure. As the foliation enters the zone, it swings towards, parallelism with the zone and some individual micas actually achieve parallelism. Then, as the foliation emerges from the other side, it curves back into its normal orientation. The sense of displacement parallel to these zones as indicated by the sense of shear of the initial foliation, is consistent with them being a system of conjugate shears related to the overall shortening of the specimen.

*Preferred orientation of salt in salt layer*

Within the pure salt layer, there is strong preferred dimensional orientation of flattened aggregates of salt. The long axes of these aggregates form a convergent fan with respect to the large fold and their orientations have been plotted on the salt layer in Fig. 7(a) where comparison with Fig. 4 shows that these orientations are parallel to the orientation of the $\lambda_1\lambda_2$-plane of the strain ellipsoid at each point in the layer (Fig. 7b).

*Preferred orientation of mica*

Some detail of the preferred orientation of mica is shown in Fig. 10 where histograms of the orientations of long axes of mica grains are given for the four regions A, B, C and D of Fig. 5. In regions A, B and C, a unimodal distribution of micas is developed reflecting the dominant long limb orientation of the kinks. The mean orientation of micas in these three regions is at 31, 27 and 35°, respectively to the local orientations of the $\lambda_1\lambda_2$-plane of strain. Within region D, in the hinge of the main fold, the distribution of micas is bimodal and the $\lambda_1\lambda_2$-plane of the strain ellipsoid bisects this distribution.

## DISCUSSION

Within the salt–mica layers, two distinct planar fabric elements have been imposed by the deformation. One consists of the axial surfaces of small kink-like folds and its distribution is presented in Fig. 7. The other consists of a preferred orientation of (001) of micas produced by tight, generally asymmetric, kinking of the initial foliation. The distribution of this preferred orientation is shown in Fig. 10. Naturally, the orientations of these two types of planar elements need not coincide, the angle between them varying between 0 and *c.* 30°. The important point illustrated by Figs. 7 and 10 is that except for the immediate hinge area of the fold, the orientation of either fabric element does not necessarily coincide with the orientation of the $\lambda_1\lambda_2$-principal plane of strain. The angle between the axial surfaces of the kinks and the $\lambda_1\lambda_2$-plane can be as great as 30° whereas the angle between the mean

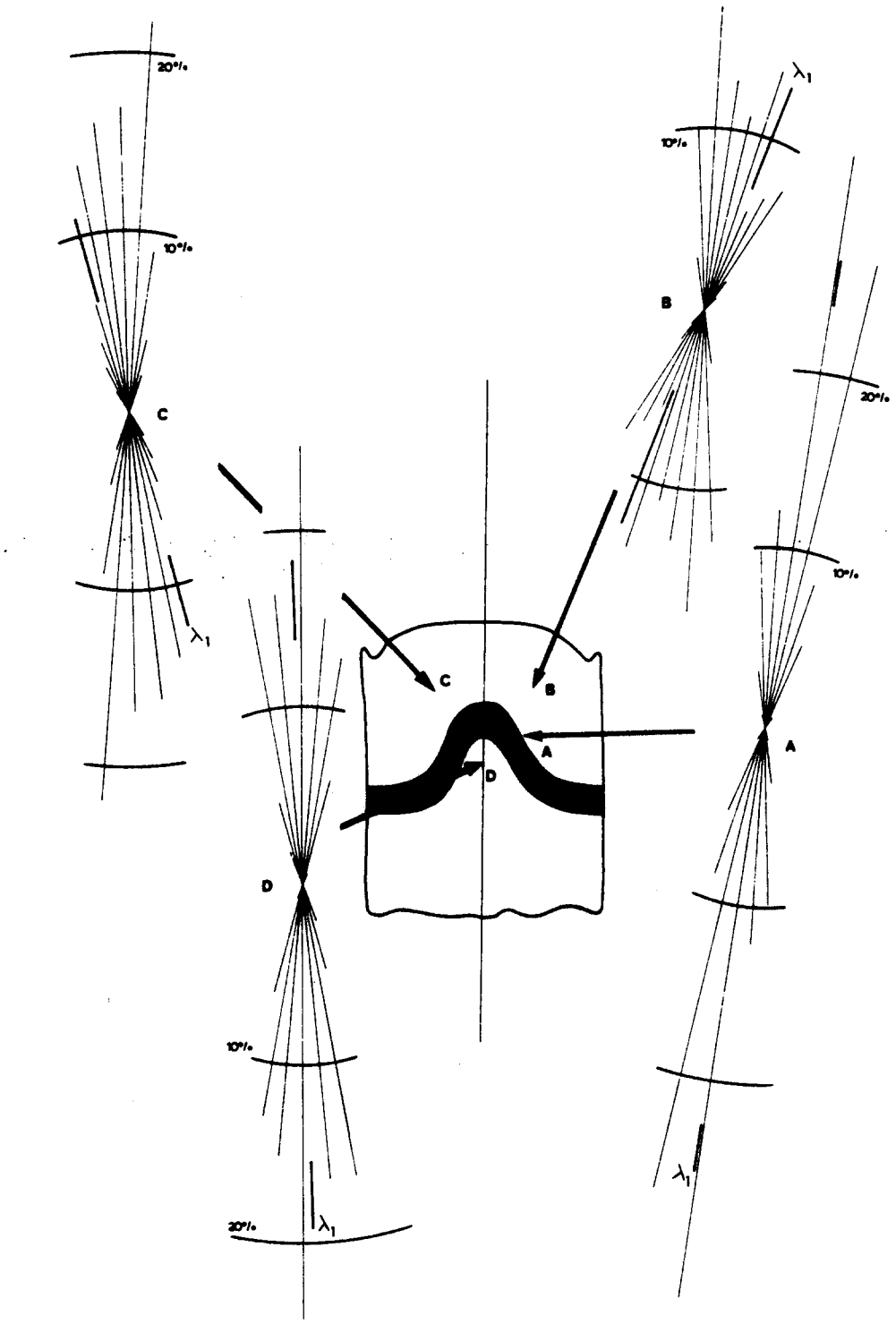


Fig. 8. Histograms showing the preferred orientation of kink boundary traces in the areas A, B, C and D of Fig. 5. The trace of the $\lambda_1\lambda_2$-principal plane of strain is also shown for each area.

preferred orientation of (001) and the $\lambda_1\lambda_2$-plane is generally greater and can be as large as 35°. These discrepancies are far greater than the errors to be expected in the orientation of the $\lambda_1\lambda_2$-plane as discussed earlier.

Thus, in the situation described by Williams *et al.* (1977) where recrystallization of micas previously oriented by tight folding is the mechanism of preferred orientation development, discordances between the foliation and the $\lambda_1\lambda_2$-plane of 35° can be expected. On the other hand, if the foliation is defined by domain boundaries as it is in crenulation cleavages and in slaty cleavage defined by small-scale crenulations (Knipe & White 1977, Weber 1981) or by fine-scale metamorphic differentiation, then discordances of 30° should not be considered unusual.

The reason that no fabric element in the salt/mica aggregates coincides with the $\lambda_1\lambda_2$-principal plane of the strain is that the deformation is inhomogeneous on a fine scale and the bulk strain is the result of combining the strains in different kinked domains within each one of which the strain is homogeneous. The strain in each small domain can be thought of as the combination of a shear

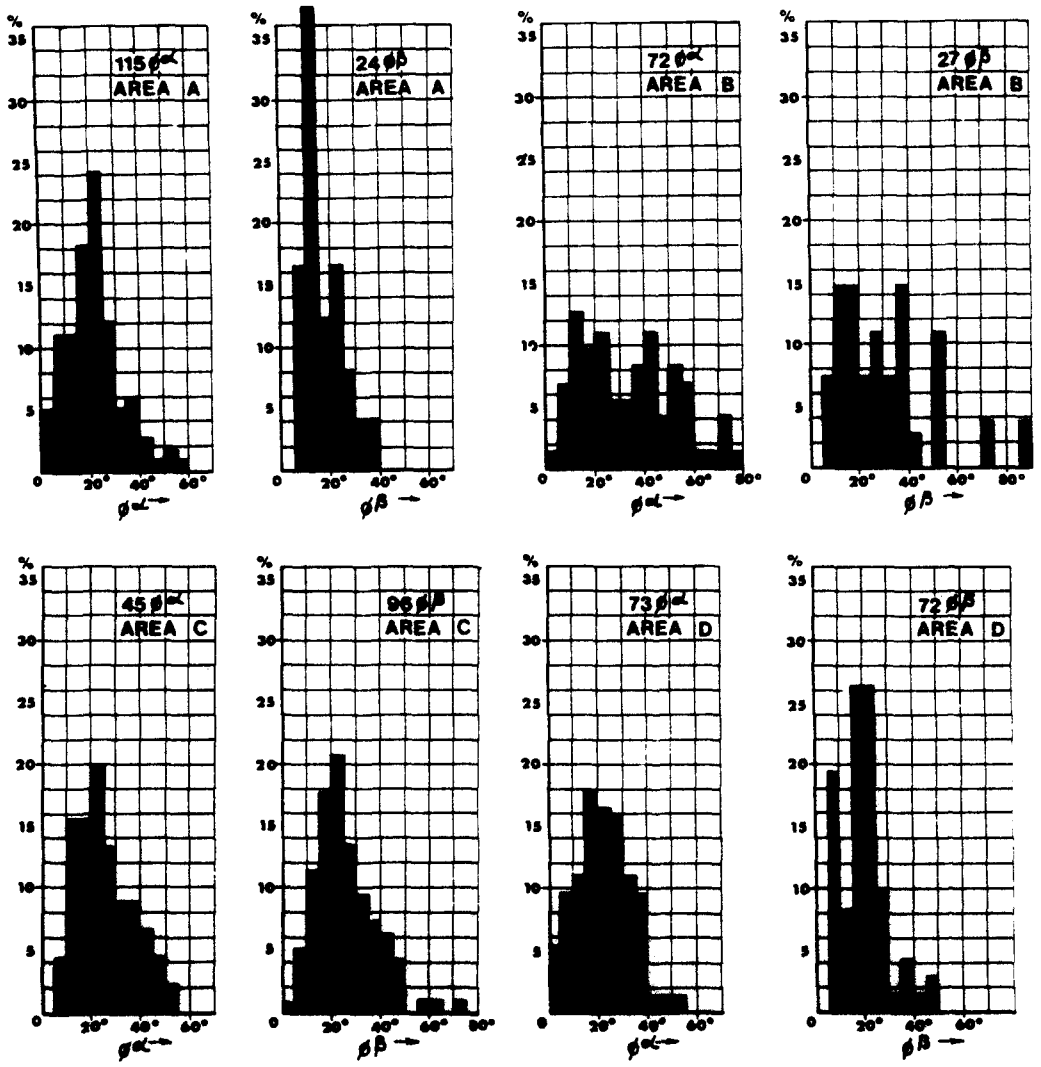


Fig. 9. Histograms showing the frequency of occurrence of kink angles $\phi^{\alpha}$, $\phi^{\beta}$ in the areas A, B, C and D of Fig. 5. These angles are defined in Fig. 11.

strain parallel to the domain boundary and a shortening normal to the domain boundary (together with a volume change that also may be different from one domain to the next). Thus, it can only be in special geometrical situations that the domain boundary or the preferred orientations of mica within a domain is parallel to the local $\lambda_1\lambda_2$-principal plane of the strain in that domain. It follows then that it can only be a special geometrical situation that leads to parallelisms of domain boundaries or of mica preferred orientation with the $\lambda_1\lambda_2$-principal plane on a scale where many different domains are combined to make a homogeneously strained area on a larger scale.

The purpose of the following discussion is to investigate the ways in which the strains in an array of homogeneously deformed domains combine to produce a homogeneously-strained region on a scale larger than the domains and to investigate the way in which the angle between the domain boundaries and the $\lambda_1\lambda_2$-principal

Table 1. Geometry of kinks in areas A B C D of Fig. 5

| Area* | Mean kink angle in domain $\alpha$(°) $\phi^{\alpha}$ | $\sigma$ | Mean kink angle in domain $\beta$(°) $\phi^{\beta}$ | $\sigma$ | Mean volume fraction of $\alpha$ $f^{\alpha}$ | Mean volume fraction of $\beta$ $f^{\beta}$ |
|---|---|---|---|---|---|---|
| A | 20.7 | 11.1 | 16.7 | 7.5 | 0.83 | 0.17 |
| B | 33.2 | 19.3 | 30.2 | 19.3 | 0.72 | 0.28 |
| C | 25.9 | 11.0 | 23.0 | 10.7 | 0.32 | 0.68 |
| D | 21.6 | 10.9 | 19.3 | 9.4 | 0.50 | 0.50 |

*139 measurements in area A; 99 measurements in area B; 141 measurements in area C and 145 measurements in area D.

(For definitions of domains $\alpha$, $\beta$ and of $\phi^{\alpha}$, $\phi^{\beta}$ see Fig. 11)

$\sigma$ is standard deviation.

plane of strain is influenced by such variables as local changes in dilation, shortening and shear strain. The general theory is developed in the Appendix and as such sets the scene for discussion of more complicated and general deformations (such as crenulation cleavage and metamorphic differentiation) than are developed in this experimental study.

*Relationship between kink boundary and principal plane of strain*

During the deformation, the small rectangle ABCD outlined by ink markers is distorted to become the parallelogram abcd as shown in Fig. 11. On a fine scale within this parallelogram, the foliation, initially parallel to AB, is inhomogeneously deformed to produce a series of kink folds, the kink boundary normals being inclined by $\theta$ to ab in the deformed state; ab is now the enveloping surface for the kink folds. The geometry of the kink system is defined in Fig. 11; the parallelogram abcd is divided into two types of domain, $\alpha$ and $\beta$, within which the foliation has more or less constant orientation. $\phi^\alpha$ and $\phi^\beta$ are the kink angles in these domains and $f^\alpha$ and $f^\beta$ are the volume fractions of the two domains.

It is shown in the appendix that the angle $\delta$ between the domain boundaries and the $\lambda_1\lambda_2$-plane of mean strain is given by

$$\sin 2\delta = \frac{2b_{12}b_{22}}{\sqrt{[(a_{11}^2 + b_{22}^2 + b_{12}^2)^2 - 4a_{11}^2 b_{22}^2]}} \quad (6)$$

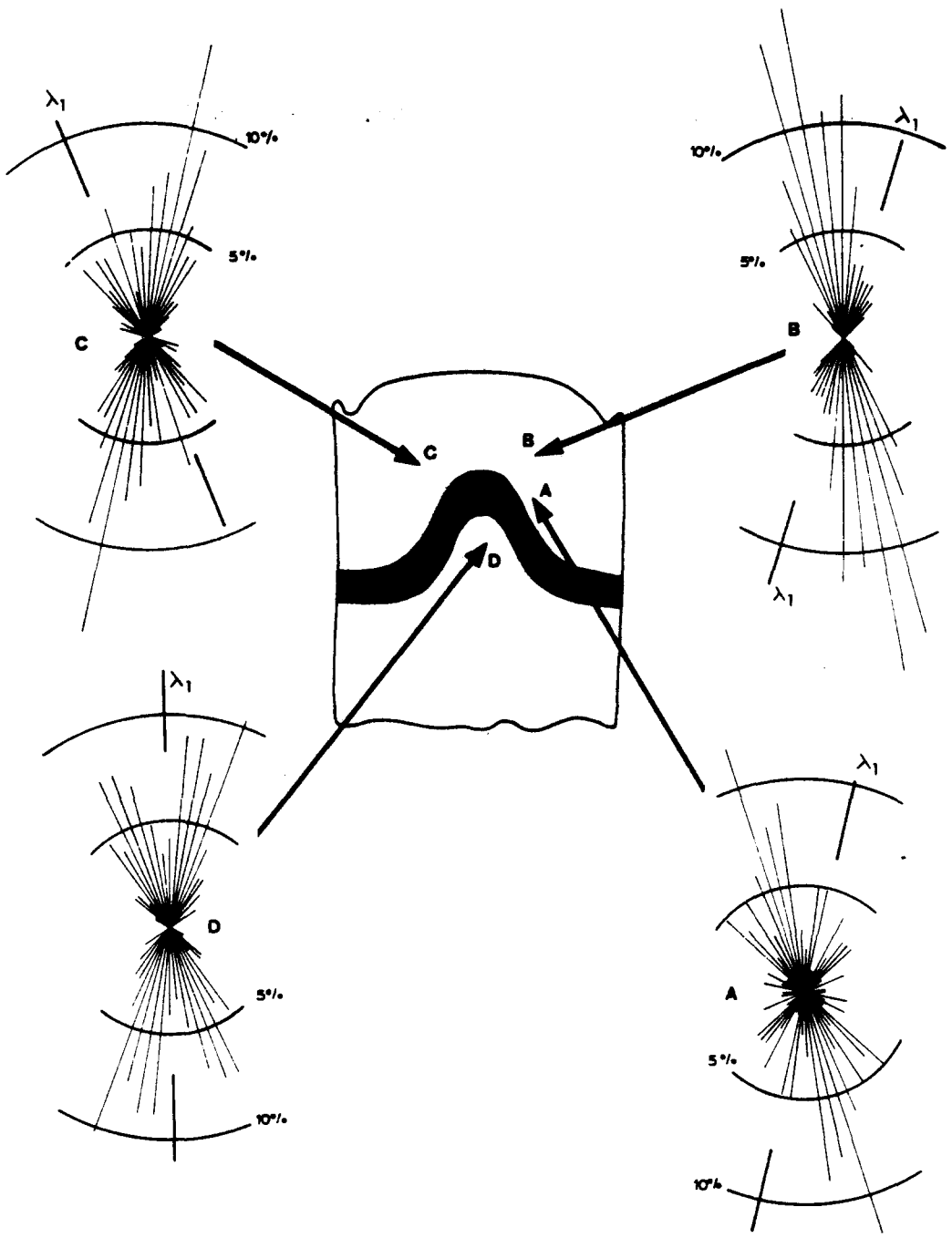


Fig. 10. Histograms showing the preferred orientation of mica (001) traces in the areas A, B, C and D of Fig. 5. The trace of the $\lambda_1\lambda_2$-principal plane of strain is also shown for each area.

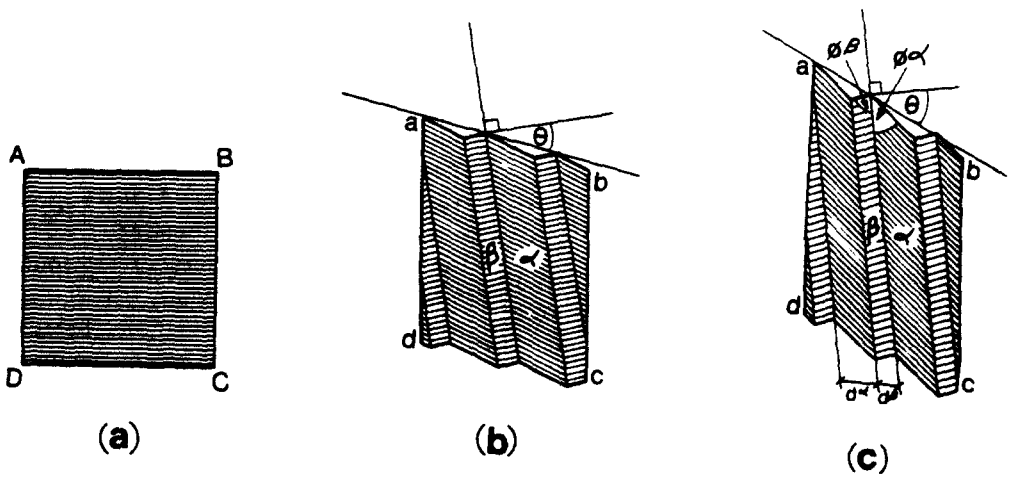


Fig. 11. (a) Undeformed square with initial foliation parallel to AB. (b) and (c) Deformed parallelograms with kinked domains $\alpha$ and $\beta$ developed on a fine scale. The kink angles in each of these domains are $\phi^{\alpha}$ and $\phi^{\beta}$, respectively and their widths are $d^{\alpha}$ and $d^{\beta}$. The kink boundary normals are inclined at $\theta$ to the enveloping surface ab.

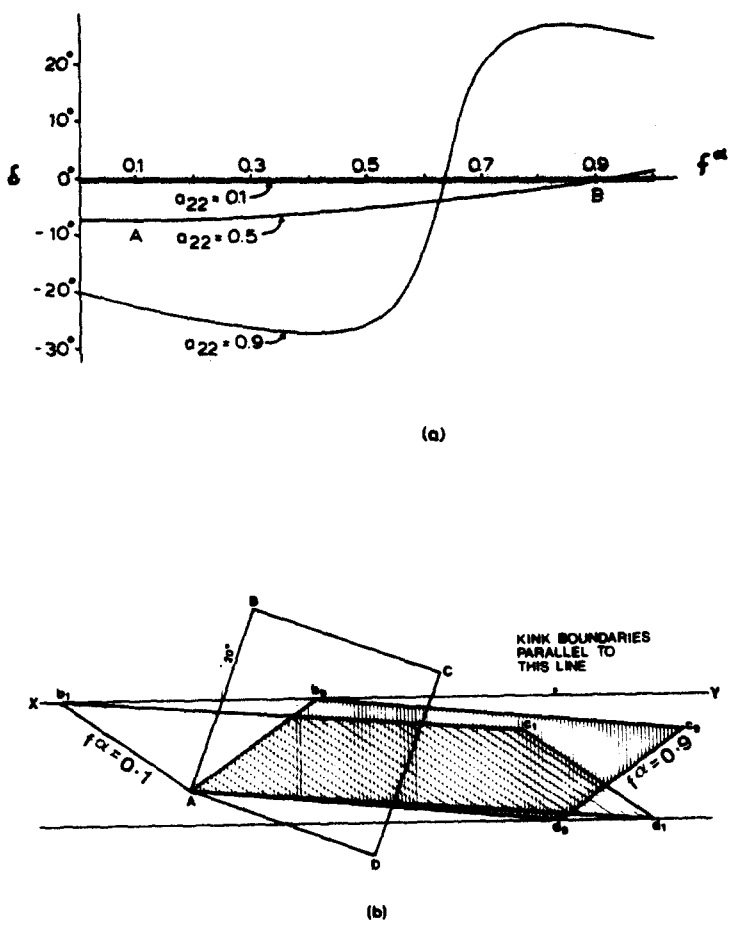


Fig. 12 (a). Variation of the angle, $\delta$, between the kink boundary and the $\lambda_1\lambda_2$-principal plane of strain with change in $f^{\alpha}$, the volume fraction of domain $\alpha$. The variation is shown for three values of the shortening normal to the kink boundary, $a_{22} = 0.1$, 0.5 and 0.9. For each case the initial angle, $\Theta$, between the foliation and the normal to the kink boundary is 20° and the kink angle is 30° in both domains. The deformation is isochoric. (b) Initial undeformed square and two extreme deformations of that square corresponding to $f^{\alpha} = 0.1$ and $f^{\alpha} = 0.9$ and $a_{22} = 0.5$ in (a), (points A and B).

where

$$b_{12} = a_{22}^{\alpha} f^{\alpha} \cot \phi^{\alpha} + a_{22}^{\beta} f^{\beta} \cot \phi^{\beta} - a_{11} \tan \Theta \quad (7)$$

and

$$b_{22} = a_{22}^{\alpha} f^{\alpha} + a_{22}^{\beta} f^{\beta}.$$

Here, $a_{11}$, $a_{22}$ are the stretches parallel to and normal to the domain boundary and $\Theta$ is the angle in the undeformed state between the normal to the foliation and the plane of material particles that will become the domain boundary. The superscripts refer to domains $\alpha$ and $\beta$.

For $\delta$ to be zero, that is, for domain boundaries to be parallel to a principal plane of strain,

$$b_{12} b_{22} = 0 \quad (8)$$

i.e. $[a_{22}^{\alpha} f^{\alpha} \cot \phi^{\alpha} + a_{22}^{\beta} f^{\beta} \cot \phi^{\beta} - a_{11} \tan \Theta] [a_{22}^{\alpha} f^{\alpha} + a_{22}^{\beta} f^{\beta}] = 0 \quad (9)$

which is not particularly illuminating. However, if we take the $a_{22}$'s in $\alpha$ and $\beta$ as always positive and non-zero then the condition for $\delta$ to be zero becomes

$$a_{22}^{\alpha} f^{\alpha} \cot \phi^{\alpha} + a_{22}^{\beta} f^{\beta} \cot \phi^{\beta} = a_{11} \tan \Theta. \quad (10)$$

The trivial case where this is true is for an isochoric deformation in each domain with equal volume fractions for domains $\alpha$ and $\beta$, with $\phi^{\alpha} = -\phi^{\beta}$ and $\Theta = 0°$.

Otherwise (10) is the general condition required for a domain boundary to be parallel to the $\lambda_1 \lambda_2$-plane of mean strain.

An example of the variation of $\delta$ for various volume fractions of the domains is given in Fig. 12(a) for $\Theta = 20°$. In these examples $\phi^{\alpha} = -\phi^{\beta} = 30°$ and the shortening normal to the domain boundary is equal in adjacent domains. The deformation is isochoric. This corresponds to symmetrical kinking in the sense that the axial plane bisects the kink fold. The following results may be read from Fig. 12:

(i) As is to be expected, with increasing shortening normal to the domain boundary the overall values of $\delta$ become smaller. Thus, for 50% shortening normal to the domain boundary ($a_{22} = 0.5$) and an initial angle of 20° between the normal to the foliation and the line of material particles that will become the domain boundary, values of $\delta$ up to just under 7° are developed. For shortening of 90% normal to the domain boundary, ($a_{22} = 0.1$), and $\Theta = 20°$, values of $\delta$ no greater than 0.2° are developed.

(ii) For $\Theta = 20°$, values of $\delta$ as high as *c.* 25° can be common. The important point is that in this situation where the folding is appressed (interlimb angle of 60°) departures of 25° are common between the domain boundary and the $\lambda_1 \lambda_2$-plane.

(iii) For the moderate strains locally developed in the experimental fold, values of $\delta$ of 20–30° are to be expected except for symmetrical situations where $\Theta = 0°$ and $f^{\alpha} = 0.5$ occur (equivalent to the hinge of the fold).

The sequence of $\delta$-values portrayed for a given value of $a_{22}$ in Fig. 12(a) corresponds to a sequence of deformations such as those shown in Fig. 12(b). This example corresponds to $a_{22} = 0.5$ where an initial square ABCD (in which the side AB, parallel to the initial foliation, lies at 20° to the normal to incipient kink boundaries) is shortened 50% normal to $XY$ as it undergoes a homogeneous simple shear parallel to $XY$. The parallelogram $Ab_1c_1d_1$ corresponds to $f^{\alpha} = 0.1$ (point A in Fig. 12a) whereas $Ab_9c_9d_9$ corresponds to $f^{\alpha} = 0.9$ (point B in Fig. 12a). Intermediate values of $f^{\alpha}$ would correspond to parallelograms intermediate between these two.

The sequence of deformations corresponding to the $a_{22} = 0.9$ curve in Fig. 12(a) are shown in Fig. 13 for $f^{\alpha} = 0.1$, 0.5 and 0.9 together with details of the kink geometry and the orientation of the strain ellipses. These deformations correspond closely to many developed in the experimental specimen.

In Fig. 14, three different situations are contrasted. Figure 14(a) is a profile of the fold showing, in summary form, the distribution of strain across the fold as determined from the distortion of marker triangles. In Fig. 14(b) the assumption is made that the foliation defined by domain boundaries is everywhere parallel to the $\lambda_1 \lambda_2$-principal plane of strain and the inferred orientations of the traces of these planes is plotted. For the most part this assumption gives the correct answer within $\pm 5°$ but locally errors of 25° are developed. Much larger errors are possible at least in principle.

In Fig. 14(c) the assumption is made that the preferred orientation of (001) of mica is everywhere parallel to the $\lambda_1 \lambda_2$-principal plane of strain except where bimodal distributions are developed when the $\lambda_1 \lambda_2$-principal plane of strain is assumed to bisect the smallest angle between the two preferred orientations of (001) of mica. Also shown in Fig. 14(c) is the value of $\sqrt{\lambda_1}$ calculated assuming that the March model is responsible for the mica preferred orientation and that the initial mica preferred orientation was random. It can be seen (cf. Figs. 14a & c) that the March model utilizing this assumption gives about the right strain magnitude but this result seems to be fortuitous since kinking of an initial strong preferred orientation is the mechanism of preferred orientation development rather than passive rotation of an initially uniform distribution of micas.

Comparison of Figs. 14(a) & (c) shows that very large errors arise from the assumptions involved but even so, the distribution and magnitudes of strain shown in Fig. 14(c) are reasonable in that they are what many workers would consider to be geologically realistic. This analysis shows however that such a criteria of 'geological realism' is by no means adequate in demonstrating that the assumptions are valid.

Examination of specimens deformed less than the present one shows that these sharp-angled folds do not form initially as conjugate kinks as in the situations described by Paterson & Weiss (1966). They form approximately normal to the local direction of shortening but from then on are progressively rotated away from parallelism with the $\lambda_1 \lambda_2$-principal plane if the history is non-coaxial until the local values of shortening normal to the kink boundary becomes appreciable when coincidence with the $\lambda_1 \lambda_2$-plane is approached again. The history of $\delta$

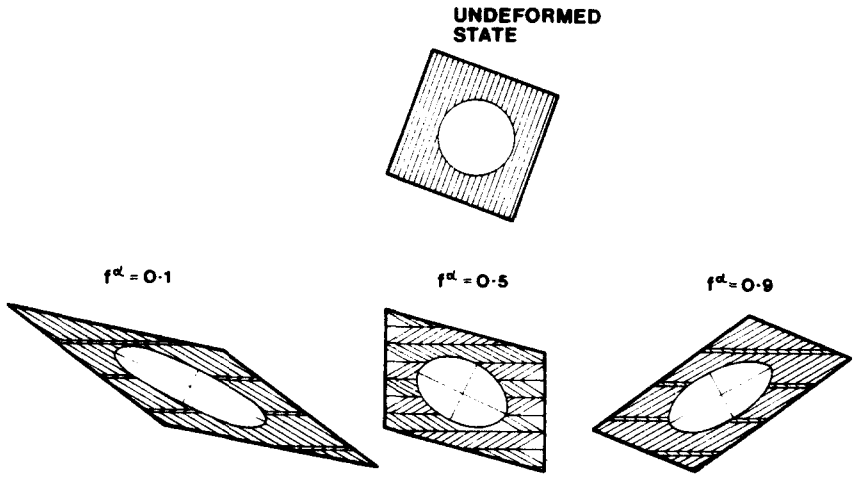


Fig. 13. Three deformed states corresponding to $f^{\alpha} = 0.1, 0.5$ and 0.9 with $a_{22} = 0.9$ in Fig. 12(a). The shapes and orientations of the strain ellipses and the deformed square are shown.

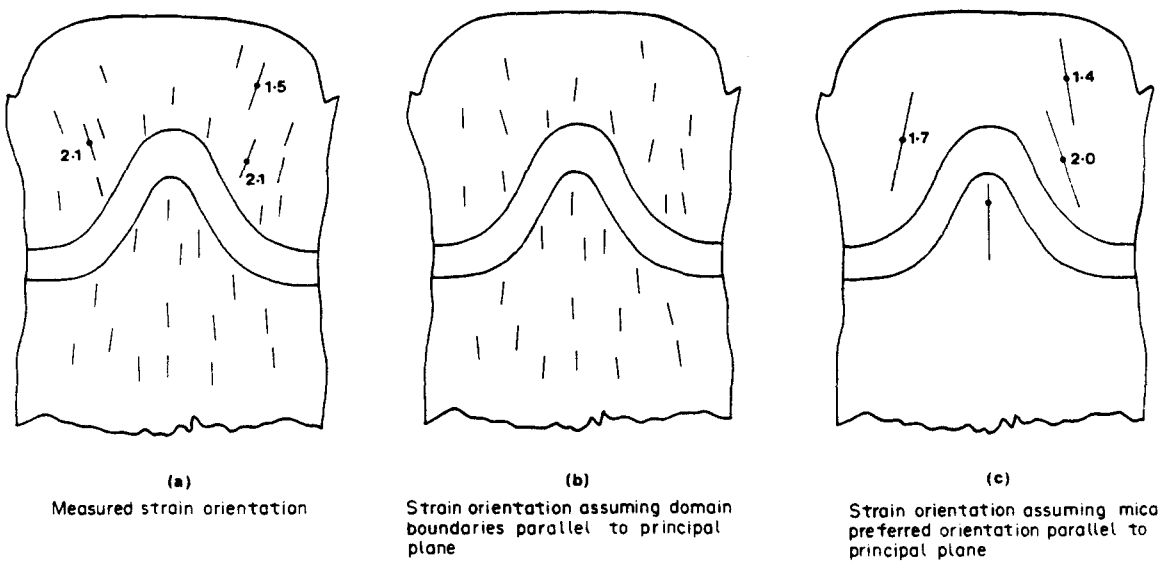


Fig. 14. (a) Measured orientation of $\lambda_1\lambda_2$-principal planes of strain in the specimen. The values of $\sqrt{\lambda_1}$ are indicated for the regions A, B and C of Fig. 5. (b) Orientation of $\lambda_1\lambda_2$-principal planes of strain assuming that kink domain boundaries are parallel to this principal plane. (c) Orientation of $\lambda_1\lambda_2$-principal planes of strain assuming that the preferred orientation of (001) of mica is parallel to this plane. The values of $\sqrt{\lambda_1}$ are shown for the regions A, B and C of Fig. 5 assuming that the preferred orientation of mica has developed by a March mechanism and that the initial fabric was random.

for a non-coaxial deformation history is, therefore, similar to that shown in Fig. 15. The history is similar to that portrayed in Hobbs *et al.* (1976 fig. 5.24).

Finally, we address the question: *for foliations that are defined by fabric discontinuities, what plane in the final strain ellipsoid does coincide with the foliation if it is not the $\lambda_1\lambda_2$-plane*? The answer is: *no plane in particular.* Geometrical parameters such as the strain and dilation in each domain and the volume fractions of each domain define a unique, but not special, orientation of the foliation with respect to the mean $\lambda_1\lambda_2$-plane and this orientation relationship in general changes as the deformation progresses. For very large shortenings normal to the domain boundaries, approximate concidence between the domain boundaries and the $\lambda_1\lambda_2$-plane may result but even for moderate strains (for instance 50% shortening) angular departures of perhaps 30° are to be expected.

*Acknowledgements*—This work was supported at various times by N.S.F. Grants GA-15918, EAR 76-03727 and EAR 8007812. We thank Alton Hajek for superb technical assistance and Dr Howard Day for computing facilities.

## REFERENCES

Bayly, M. B. 1974. Cleavage not parallel to finite-strain ellipsoid's XY plane: discussion. *Tectonophysics* **23**, 205–207.

Becker, G. F. 1893. Finite homogeneous strain, flow and rupture of rocks. *Bull. geol. Soc. Am.* **4**, 13–90.

Cobbold, P. R. 1977. Description and origin of banded deformation

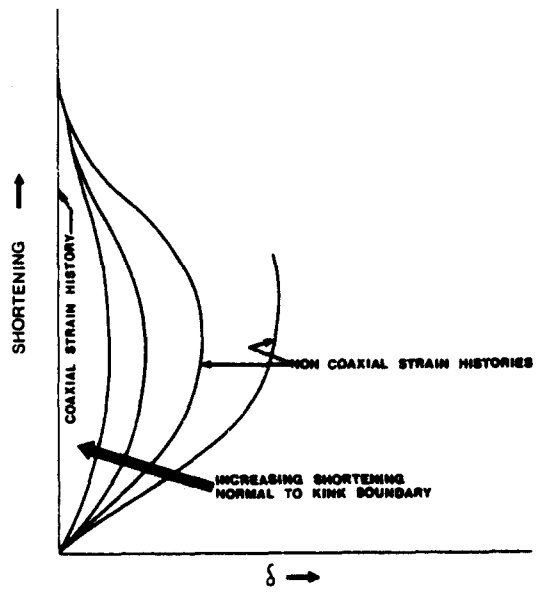


Fig. 15. History for the angle $\delta$, between a kink boundary and the $\lambda_1\lambda_2$-principal plane of strain for increasing strain. The various curves are for non-coaxial histories and represent various components of shortening normal to the kink boundary.

structures. I. Regional strain, local perturbations, and deformation bands. *Can. J. Earth Sci.* **14**, 1721–1731.
Darwin, C. 1846. Geological observations on South America. In: *Coral Reefs, Volcanic Islands, South American Geology*, Ward Lock, London, 1910.
Etheridge, M. A. & Lee, M. F. 1975. Microstructures of slates from Lady Loretta, Queensland, Australia. *Bull. geol. Soc. Am.* **86**, 13–22.
Harker, A. 1885. On slaty cleavage and allied rock structure with special reference to the mechanical theories of their origin. *Rep. Br. Ass. Advmt Sci.* 1855, 813–852.
Hobbs, B. E. 1971. The analysis of strain in folded layers. *Tectonophysics* **11**, 239–375.
Hobbs, B. E., Means, W. D. & Williams, P. F. 1976. *An Outline of Structural Geology*. Wiley, New York.
Hoeppener, R. 1956. Zum problem der Bruchbildung, Schiefering und Faltung. *Geol. Rdsch.* **45**, 247–283.
Knipe, R. J. & White, S. H. 1977. Microstructural variation of an axial plane cleavage around a fold — a H.V.E.M. study. *Tectonophysics* **39**, 355–380.
Means, W. D. 1975. Natural and experimental microstructures in deformed micaceous sandstones. *Bull. geol. Soc. Am.* **86**, 1211–1229.
Means, W. D. 1976 *Stress and Strain, Basic Concepts of Continuum Mechanics for Geologists*. Springer, New York.
Means, W. D. 1977. Experimental contributions to the study of foliations in rocks: a review of research since 1960. *Tectonophysics* **39**, 329–354.
Means, W. D. & Williams, P. F. 1972. Crenulation cleavage and faulting in an artificial salt-mica schist. *J. Geol.* **80**, 569–591.
Means, W. D., Williams, P. F. & Hobbs, B. E. in press. Progressive

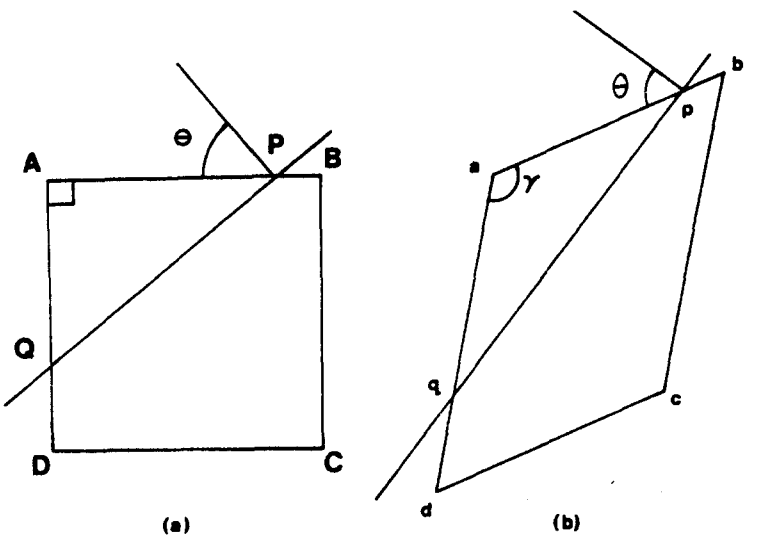


Fig. 16 (a) Undeformed square A B C D with initial foliation parallel to AB. PQ is a line of material particles that will define the trace of the kink boundary in the deformed state. $\Theta$ is the initial angle between the foliation and the normal to PQ. (b) Deformed parallelogram a b c d. The right angle BAC has become $\gamma$. pq is the trace of the kink boundary in the deformed state. $\theta$ is the angle between the enveloping surface ab and the normal to pq.

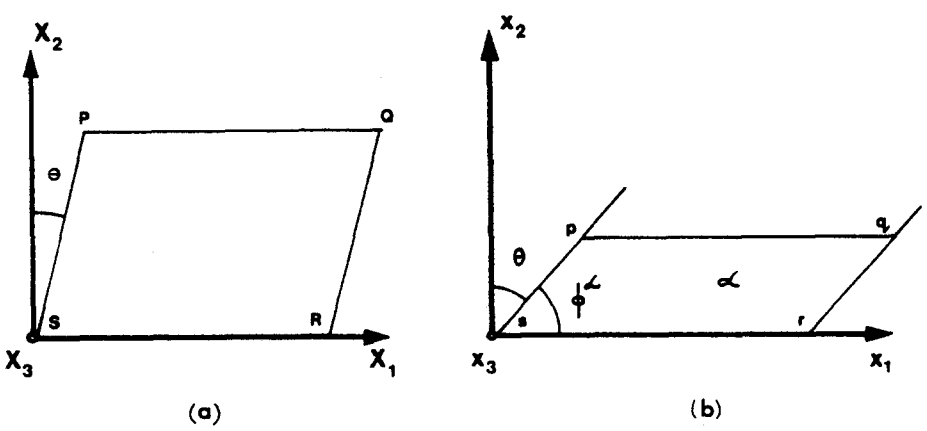


Fig. 17. Deformation of a single kink domain P Q R S to become p q r s.

deformation and fabric development in experimentally folded salt–mica specimens. *J. geophys. Res.*
Paterson, M. S. & Weiss, L. E. 1966. Experimental deformation and folding in phyllite. *Bull. geol. Soc. Am.* **77**, 343–373.
Plessmann, W. von 1964. Gesteinlosung, ein Hauptfaktor beim Schieferungsprozess. *Geol. Mitt.* **4**, 69–82.
Ramsay, J. G. 1967. *Folding and Fracturing of Rocks.* McGraw-Hill, New York.
Ramsay, J. G. & Graham, R. H. 1970. Strain variation in shear belts. *Can. J. Earth Sci.* **7**, 786–813.
Siddans, A. W. B. 1972. Slaty cleavage — a review of research since 1815. *Earth Sci. Rev.* **8**, 205–232.
Sorby, H. C. 1853. On the origin of slaty cleavage. *Edinb. New Philos. J.* **55**, 137–148.
Talbot, J. L. 1965. Crenulation cleavage in the Hansruckschiefer of the Middle Moselle region. *Geol. Rdsch.* **54**, 1026–1043.
Truesdell, C. & Toupin, R. 1960. *The Classical Field Theories.* Encyclopedia of Physics, Volume 3 (1) (edited by Flugge, S.,). Springer Berlin, 226–793.
Weber, K. 1981. Kinematic and metamorphic aspects of cleavage formation in very low-grade metamorphic slates. *Tectonophysics* **78**, 291–306.
Williams, P. F. 1972. Development of metamorphic layering and cleavage in low grade metamorphic rocks at Bermagui, Australia. *Am. J. Sci.* **272**, 1–47.
Williams, P. F. 1976. Relationships between axial plane foliations and strain. *Tectonophysics* **30**, 181–186.
Williams, P. F. 1977. Foliation: a review and discussion. *Tectonophysics* **39**, 305–328.
Williams, P. F., Means, W. D. & Hobbs, B. E. 1977. Development of axial plane slaty cleavage and schistosity in experimental and natural materials. *Tectonophysics* **42**, 139–158.
Wood, D. S. 1974. Current views of the development of slaty cleavage. *A. Rev. Earth Planet. Sci.* **2**, 1–35.
Wood, D. S., Oertel, G. Singh, J. & Bennett, H. F. 1976. Strain and anisotropy in rocks. *Phil. Trans. R. Soc. Lond.* **A283**, 27–42.

## APPENDIX

The aim of this appendix is to define the relationship between the orientation of the $\lambda_1\lambda_2$-principal plane of strain, for a statistically homogeneous deformation comprised of small planar domains of different strain, and the domain boundaries for various geometrical features of the domains.

*Strain in a single domain*

In Fig. 16(a) the undeformed situation is illustrated where an incipient kink plane, PQ, is shown developing with its normal at an angle $\Theta$ to the foliation AB. In the deformed state (Fig. 16b) the kink plane normal makes an angle $\theta$ with the enveloping surface, ab. The initial right angle PAQ has become $\gamma$. Since the deformation is homogeneous, AP : AB = ap : ab and AQ : AD = aq : ad. Therefore,

$$\text{AQ:AP} = \cot\Theta = (\text{aq:ap})\,(\text{AD:ad})\,(\text{ab:AB}), \tag{A1}$$

or

$$\cot\Theta = \frac{\cos\theta}{\cos(\gamma-\theta)}\cdot\frac{S_{ab}}{S_{ad}} \tag{A2}$$

where $S_{ab}$, $S_{ad}$ are the stretches in the directions of ab and ad, respectively.

We adopt systems of Cartesian coordinates $X_1$, $X_2$ and $X_3$ in the undeformed state and $x_1$, $x_2$ and $x_3$ in the deformed state with $X_1$, $x_1$ parallel to the kink plane, but normal to the kink axis, $X_2$, $x_2$ normal to the kink plane and $X_3$, $x_3$ parallel to the kink axis (Fig. 17). During deformation, $X_3$, $x_3$ are principal axes of strain and a particular domain undergoes a progressive homogeneous shear parallel to the kink boundary coupled with a homogeneous shortening parallel to $x_2$ and a homogeneous extension parallel to $x_1$, accomplished mainly by the deformation of salt aggregates between the mica flakes. The deformation for domain $\alpha$ may, therefore, be written as the following equation relating the deformed and undeformed coordinates of a particle:

$$x_1 = a_{11}X_1 + a_{12}X_2 \tag{A3}$$

$$x_2 = a_{22}X_2$$

$$\text{where } a_{12} = a_{22}\tan\theta - a_{11}\tan\Theta \tag{A4}$$

$$= a_{22}\cot\phi^\alpha - a_{11}\tan\Theta$$

and $a_{11}$, $a_{22}$ are the stretches parallel to $x_1$ and $x_2$, respectively in the domain $\alpha$.

The strain relative to the deformed state is given by the inverse, $\bar{c}^1$ of Cauchy's tensor (see Truesdell & Toupin 1960, p. 263, Hobbs 1971):

$$\bar{c}^1_{ij} = \delta_{IJ}\frac{\partial xi}{\partial X_I}\frac{\partial xj}{\partial X_J} \tag{A5}$$

where $\delta_{IJ}$ is the Kronecker delta.

So that

$$\bar{c}^1_{11} = a^2_{11} + a^2_{12}$$

$$\bar{c}^1_{12} = a_{12}a_{22} \tag{A6}$$

$$\bar{c}^1_{22} = (a_{22})^2 .$$

The principal quadratic elongations are given by the roots of

$$\begin{bmatrix} \bar{c}^1_{11}-\lambda & \bar{c}^1_{12} \\ \bar{c}^1_{12} & \bar{c}^1_{22}-\lambda \end{bmatrix} = 0 \tag{A7}$$

or

$$\lambda^2 - \lambda[a^2_{11} + a^2_{22} + a^2_{12}] + a^2_{11}a^2_{22} = 0 \tag{A8}$$

$$\therefore \lambda = \{[a^2_{11} + a^2_{22} + a^2_{12}]$$

$$\pm\sqrt{[(a^2_{11} + a^2_{22} + a^2_{12})^2 - 4a^2_{11}a^2_{22}]}\}/2 \tag{A9}$$

and the principal stretches are the square roots of each $\lambda$.

Again, the angle, $\delta$, between the principal stretch and the $x_1$-axis is given by

$$\sin 2\delta = \frac{2\bar{c}^1_{12}}{\bar{c}^1_1 - \bar{c}^1_2} \tag{A10}$$

where $\bar{c}^1_1$ and $\bar{c}^1_2$ are the principal quadratic elongations (given by the two values of $\lambda$ in A9).

Hence

$$\sin 2\delta = \frac{2a_{12}a_{22}}{\sqrt{[(a^2_{11} + a^2_{22} + a^2_{12})^2 - 4a^2_{11}a^2_{22}]}}. \tag{A11}$$

The dilation in the domain due to the deformation is

$$\Delta = a_{11}a_{22} . \tag{A12}$$

*Compatibility of strain between domains*

For each of the domains $\alpha$ and $\beta$ in Fig. 11 we can write down transformations identical to (A3) and a deformation tensor given by (A6). We can also calculate the values of the principal quadratic elongations in each domain from (A9) and the angle between the kink plane and the maximum principal stretch in each domain from (A11).

Since continuity is maintained across the kink plane boundary,

$$a^\alpha_{11} = a^\beta_{11} \tag{A13}$$

where the superscripts refer to individual domains.

Also, the dilation in each domain is given by an expression such as (A12). So, combining (A12) and (A13)

$$a^\alpha_{22}\Delta^\beta = a^\beta_{22}\Delta^\alpha. \tag{A14}$$

Also, if $\Delta$ is now written as the dilation of the specimen as a whole and $d^\alpha$, $d^\beta$ are the widths of $\alpha$ and $\beta$, then

$$\Delta = f^\alpha\Delta^\alpha + f^\beta\Delta^\beta \tag{A15}$$

$$\text{where } f^\alpha = d^\alpha/(d^\alpha + d^\beta)$$

$$\text{and } f^\beta = d^\beta/(d^\alpha + d^\beta). \tag{A16}$$

*Mean deformation due to array of domains*

The problem of determining the mean strain from an array of fine-scale homogeneously deformed domains has been treated by Cobbold (1977) from which we obtain the following transformation describing the mean deformation after using (A3) and (A4):

$$x_1 = a_{11}X_1 + [a^\alpha_{22}f^\alpha\cot\phi^\alpha + a^\beta_{22}f^\beta\cot\phi^\beta - a_{11}\tan\Theta]X_2$$

$$x_2 = [a^\alpha_{22}f^\alpha + a^\beta_{22}f^\beta]X_2. \tag{A17}$$

If we put $b_{12} = a^\alpha_{22}f^\alpha\cot\phi^\alpha + a^\beta_{22}f^\beta\cot\phi^\beta - a_{11}\tan\Theta$ (A18)

and $b_{22} = a_{22}^{\alpha} f^{\alpha} + a_{22}^{\beta} f^{\beta}$.

Then (A17) becomes

$$x_1 = a_{11} X_1 + b_{12} X_2$$
$$x_2 = b_{22} X_2, \text{ similar to (A3)} \tag{A19}$$

and the principal quadratic elongations for the region as a whole and the angle between the kink planes and the principal stretch, $\delta$, can be obtained using (A9) and (A11).

In particular,

$$\sin 2\delta = \frac{2 b_{12} b_{22}}{\sqrt{[(a_{11}^2 + b_{22}^2 + b_{12}^2)^2 - 4 a_{11}^2 b_{22}^2]}}. \tag{A20}$$